

05 Aug 2010

Structural Measurements for Enhanced MAV Flight


John R. Singler

Missouri University of Science and Technology, singlerj@mst.edu

Gregg Abate

Benjamin T. Dickinson

Follow this and additional works at: https://scholarsmine.mst.edu/math_stat_facwork

 Part of the [Mathematics Commons](#), and the [Statistics and Probability Commons](#)

Recommended Citation

J. R. Singler et al., "Structural Measurements for Enhanced MAV Flight," *Proceedings of the AIAA Atmospheric Flight Mechanics Conference (2010, Toronto, ON, Canada)*, American Institute of Aeronautics and Astronautics (AIAA), Aug 2010.

The definitive version is available at <https://doi.org/10.2514/6.2010-7933>

This Article - Conference proceedings is brought to you for free and open access by Scholars' Mine. It has been accepted for inclusion in Mathematics and Statistics Faculty Research & Creative Works by an authorized administrator of Scholars' Mine. This work is protected by U. S. Copyright Law. Unauthorized use including reproduction for redistribution requires the permission of the copyright holder. For more information, please contact scholarsmine@mst.edu.

Structural Measurements for Enhanced MAV Flight

Ben Dickinson*

Air Force Research Laboratory, Munitions Directorate, Eglin AFB, FL 32542

John R. Singler,†

Department of Mathematics and Statistics, Missouri University of Science and Technology, Rolla, MO 65409

Gregg Abate,‡

Air Force Research Laboratory, Munitions Directorate, Eglin AFB, FL 32542

Our sense of touch allows us to feel the forces in our limbs when we walk, swim, or hold our arms out the window of a moving car. We anticipate this sense is key in the locomotion of natural flyers. Inspired by the sense of touch, the overall goal of this research is to develop techniques for the estimation of aerodynamic loads from structural measurements for flight control applications. We submit a general algorithm for the direct estimation of distributed steady loads over bodies from embedded noisy deformation-based measurements. The estimation algorithm is applied to a linearly elastic membrane test problem where three applied distributed loads are estimated using three measurement configurations with various amounts of noise. We demonstrate accurate load estimates with simple sensor configurations, despite noisy measurements. Online real-time aerodynamic load estimates may lead to flight control designs that improve the stability and agility of micro air vehicles.

I. Introduction

The Air Force Research Laboratory has a keen interest in the development of micro air vehicles (MAVs) for use in military applications such as reconnaissance, situational awareness, precision payload delivery, and aid in rescue. Although the smaller size^a of MAVs makes them ideal for easy transportation and flight in urban environments, their scale also leads to new challenges in flight mechanics and control. MAVs can be considered a sub-class of larger scale unmanned air vehicles (UAVs). UAVs have been developed in recent years by leveraging traditional aerospace science technologies. However, the engineering maturity required for MAV development has not kept pace. For instance, due to low Reynolds number regimes of flight ($Re \sim 10^5$ or less), their flow fields often experience separated flow regimes on the order of the vehicle size. The small size of MAVs also gives rise to small inertias which make the MAV more susceptible to wind gusts (Figures 1 and 2).¹

The MAV flight mechanics challenge consists of generating sufficient power to maneuver; negotiating gusts while keeping sensors on target; remaining controllable despite ground effects or the presence of other obstacles; precisely maintaining path and orientation in confined spaces; perching and performing related maneuvers of precision landing; and achieving all of these with minimal onboard energy, low resolution noisy measurements, and with limited onboard computational resources.³ In combination with aircraft design, these challenges will be met with various guidance and control strategies.

The various sensing modalities observed in biological systems lead us to consider the integration of bioinspired sensors for control. One example is structural feedback. In the same way that we can feel the forces in our limbs when we walk, swim, or hold our arms out the window of a moving car, we anticipate that natural flyers feel the aerodynamic loads on their wings and that this sense plays a significant role in their stable yet agile flight. To exploit this sense in MAV's, our goal is to develop methods for processing distributed

*Mechanical Engineer, AFRL/RWGN, 101 W Eglin Blvd; Eglin AFB, FL 32542; AIAA Member.

†Assistant Professor, Missouri University of Science and Technology; Rolla, MO 65409.

‡Aerospace Engineer, AFRL/RWGN, 101 West Eglin Blvd; Eglin AFB, FL 32542; AIAA Associate Fellow.

^aMaximum dimensions on the order of 10cm

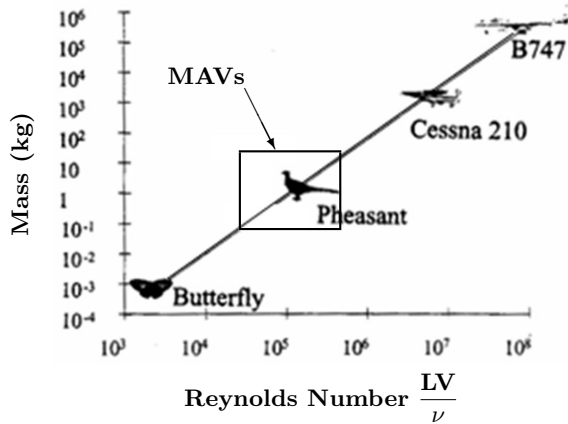


Figure 1. Mass versus Reynolds number for MAVs²



Figure 2. Examples of MAVs

structural measurements for engineering applications. Although the concept of structural measurement may be bioinspired, the existing framework of model-based control design is not. Instead of emulating the biological control system, we aim to translate the role of structural feedback in biological systems to engineered control system designs (see also reference 4).

Following the role we infer for the sense of touch in natural flyers, the goal of this effort is to determine how structural information can provide a sense of the aerodynamic forces on a body. Since model-based control designs operate on physical quantities (forces, moments, rotation rates, velocity, etc.) we will develop a general algorithm to quantify distributed loads from a limited set of structural measurements.

The problem of determining a distributed load over a structure from limited measurements (e.g., displacements or strains) is an inverse problem and has been previously studied by many researchers for various purposes. In the analysis of real structures, applied loads are often difficult to characterize which limits the accuracy of finite element analysis (FEA). For improved FEA of structures, Chock⁵ approximated distributed loads on a 1D beam using a finite element discretization and the steepest descent method. Li⁶ also provided a comprehensive study of load estimation over a one dimensional beam and a three dimensional truss using FEA and iterative methods. Maniatty⁷ has approximated solutions of inverse elasticity problems to better estimate stress, strain or displacement fields from limited noisy experimental data.

The identification of real-time flight loads is also important in the field of structural health monitoring. For this purpose, Coates⁸ created a database composed of the Fourier coefficients of a set of 5 candidate or “historical” loads, then used least squares methods based on strain measurements to select the coefficients from the database that best matched an unknown applied steady load. Shkarayev⁹ also used least squares methods to estimate the coefficients of polynomial loads over a cantilevered plate and aircraft wing box with strain data. White¹⁰ explored load estimation over cantilever beams for wind turbine applications. In an effort closely related to this study, Stanford¹¹ has estimated aerodynamic pressure fields over a membrane MAV wing using experimentally determined displacement fields.

We note that two procedural steps are common to the above studies: 1) the discretization of the structural system (except White¹⁰ which was analytical) and an *a-priori* parameterization of the load, and 2) the identification of the load parameters with least squares methods or iterative procedures. With this approach the accuracy of the estimated load is discretization dependent, as clearly demonstrated by Li.⁶ Additionally, the parameterization of the load is ad-hoc. There is no way in advance to tell if a particular parameterization of the load will lead to a successful estimate.

To avoid such numerical uncertainty, we take a different approach. Here, we develop an algorithm to approximate solutions to the inverse load estimation problem at the infinite dimensional level (the PDE level), and only discretize to recover the load estimate. With this approach, the estimated load is essentially discretization independent and we can obtain an exact form of the estimated load. In this paper we will 1) present a general load estimation problem statement, 2) develop a general method for distributed load estimation for structures in equilibrium from deformation-based measurements, and 3) demonstrate accurate load estimation for a linear membrane test problem from limited noisy structural measurements.

II. Problem Definition

Consider a solid body immersed in an arbitrary flow environment, where a finite set of integrated external or internal structural measurements^b are made (Figure 3). At any instant, from the set of structural

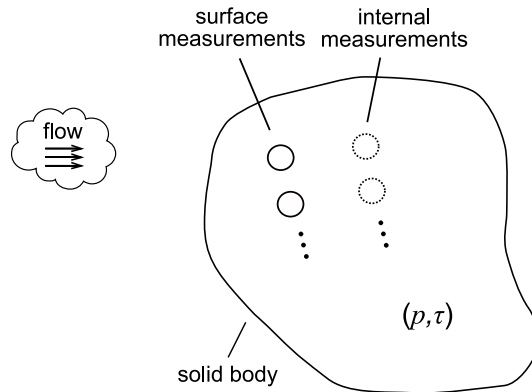


Figure 3. Illustration of the general problem, to find the best estimate of surface forces given a limited set of structural measurements

measurements we wish to find the best estimate of surface forces on the body, that is, the pressure p , and shear stress τ .

As discussed in the introduction, we are interested in load estimation for MAV control designs; therefore, wings are our structures of interest. In this work we present an algorithm for a specialization of the above problem: linearly elastic structures in equilibrium. Specifically, the load estimation algorithm developed herein is valid for structural systems described by elliptic partial differential equations. We test the load estimation algorithm on an linear elastic membrane problem. Details of the membrane problem are presented in the following section.

III. Membrane Problem

The specific problem we consider is the estimation of a distributed load applied over a linearly elastic structure in equilibrium. Our test problem is a circular membrane with radius R , where a set of structural measurements are locally taken over regions $S_i \subset \Omega$ for $i = 1, \dots, m$. Following Stanford,^{11,12} we use the

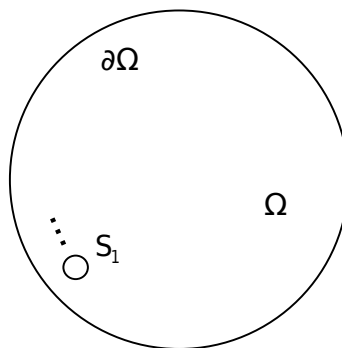


Figure 4. Diagram of circular membrane with embedded structural measurements taken over circular subsets of Ω

following equation describing the transverse displacement of a prestrained membrane with zero Dirichlet

^bWe define *structural measurements* as information derived from the deformation of the body.

boundaries,

$$N_{xx} \frac{\partial^2 w}{\partial x^2} + 2 N_{xy} \frac{\partial^2 w}{\partial x \partial y} + N_{yy} \frac{\partial^2 w}{\partial y^2} = -f, \quad (x, y) \in \Omega \quad (1)$$

$$w(\partial\Omega) = 0,$$

where w represents transverse membrane displacement, f is an applied distributed load (e.g. a pressure field), and the tensor

$$N = \begin{bmatrix} N_{xx} & N_{xy} \\ N_{xy} & N_{yy} \end{bmatrix}$$

represents in-plane prestresses, determined from the following constitutive equation for the plane stress state

$$\begin{bmatrix} N_{xx} \\ N_{yy} \\ N_{xy} \end{bmatrix} = \frac{E t}{1 - \nu^2} \begin{bmatrix} 1 & \nu & 0 \\ \nu & 1 & 0 \\ 0 & 0 & (1 - \nu) \end{bmatrix} \begin{bmatrix} \epsilon_{xx}^0 \\ \epsilon_{yy}^0 \\ \epsilon_{xy}^0 \end{bmatrix}. \quad (2)$$

In equation (2), E is Young's modulus, ν is Poisson's ratio, t is the membrane thickness, and $[\epsilon_{xx}^0, \epsilon_{yy}^0, \epsilon_{xy}^0]$ in the right hand side of the constitutive equation (2) represent prestrain fields. In the prestrain condition, if the membrane experiences zero net pressure and volume forces are assumed negligible, it follows from Cauchy's theorem for an elastic body that the divergence of N is zero. For this computational investigation, $N_{xx} = 2, N_{xy} = -1, N_{yy} = 2$ (to ensure the problem is coercive, see Section IV.A, and N is divergence free).

The following measurements are made over the membrane,

$$y_i = \int_{\Omega} g_i w_x d\mathbf{x} + \eta_i, \quad \text{for } i = 1, \dots, m, \quad (3)$$

$$y_i = \int_{\Omega} g_i w_y d\mathbf{x} + \eta_i, \quad \text{for } i = m + 1, \dots, 2m \quad (4)$$

where

$$g_i = \begin{cases} 1 & \text{if } (x, y) \in S_i \\ 0 & \text{otherwise} \end{cases}$$

for $i = 1, \dots, m$ and each η_i is zero-mean, Gaussian, white noise. Each measurement location S_i supplies two signals which may be physically interpreted as accumulated displacements in the x and y directions over each region, respectively. Each region S_i is circular with a diameter of $0.04 R$.

In physical applications, strain appears the most likely measurement quantity. However, the above membrane model (1) is not ideal for such measurements. Our previous load estimation studies for an Euler-Bernoulli beam show that with suitably derived algorithms, both strain and displacement-type measurements are effective for load estimation. We anticipate that strain measurements for the membrane problem (provided strain measurements are computable from the model) or any other suitable structure, will provide estimates of similar accuracy to those computed from the displacement-type measurements herein. We plan to explore this issue further in future work.

Finally, we note that a physical presence of the measurements described here is not included in the structural description. The integration of actual sensors into a structure, with material properties different than the structure itself, can significantly affect structural behavior.¹³ Beyond proof-of-principle tests, the material discontinuities of embedded sensors should be accounted for in the constitutive equation (2).

III.A. Weak form of the membrane equation

The development of the load estimation algorithm is based on a variational or weak form of the governing equation (1). Since N is divergence free, it can be checked that the PDE (1) is equivalent to

$$-\nabla \cdot (N \nabla w) = f. \quad (5)$$

The weak form of (5) is obtained by multiplying through by a test function, v , and integrating by parts. This leads to the following problem: to find the displacement field $w(x, y) \in V = \{v \in H^1(\Omega) | v(\partial\Omega) = 0\}$

such that

$$a(w, v) \equiv \int_{\Omega} N_{xx} \frac{\partial w}{\partial x} \frac{\partial v}{\partial x} + N_{xy} \frac{\partial w}{\partial x} \frac{\partial v}{\partial y} + N_{xy} \frac{\partial w}{\partial y} \frac{\partial v}{\partial x} + N_{yy} \frac{\partial w}{\partial y} \frac{\partial v}{\partial y} d\mathbf{x} = \int_{\Omega} f v d\mathbf{x}, \quad (6)$$

for all $v \in V$, where the space H^1 contains all square integrable functions whose x and y partial derivatives are square integrable. Also, note that the zero boundary conditions are included in the space V . Equation (6) may also be written as $a(w, v) = (f, v)_{L^2}$, where $a : V \times V \rightarrow \mathbb{R}$ and $(f, v)_{L^2} = \int_{\Omega} f v d\mathbf{x}$ is the standard L^2 inner product.

Furthermore, the measurement model can be represented $y_i = C_i w$, where $C_i w$ is given in (4).

IV. Load Estimation Algorithm

In this section, we describe the load estimation algorithm for a general class of elliptic partial differential equations. The membrane load ID problem described above is an example of a problem in this class. We describe the algorithm in general since many other load estimation problems can be placed in this form. We give the general framework in Section IV.A, describe the load estimation inverse problem in Section IV.B, and present the algorithm in Section IV.C.

We develop the problem and algorithm at the PDE level and then discretize to obtain the load estimate. This contrasts with the alternative approach of first discretizing the problem and then developing the algorithm at the discrete level. We believe the approach we take in this work has potential to offer many advantages over the alternative approach. We discuss this in detail in Section IV.C.

After Section IV.A, readers primarily interested in the algorithm and implementation details may directly refer to the load estimation problem statement (10) and its solution algorithm in Section IV.C without lack of continuity.

IV.A. General Problem Framework

Let H and V be two real Hilbert spaces with inner products $(\cdot, \cdot)_H$ and $(\cdot, \cdot)_V$ and corresponding norms $\|f\|_H = (f, f)_H^{1/2}$ and $\|g\|_V = (g, g)_V^{1/2}$. Assume V is continuously embedded in H , i.e., V is a dense subspace of H and there is a positive constant C_V such that $\|v\|_H \leq C_V \|v\|_V$ for all v in V .

We consider the variational form of the PDE model as follows. Let $a : V \times V \rightarrow \mathbb{R}$ be a real-valued bilinear form that is bounded and V -elliptic, i.e., there are positive constants c_0 and C_0 such that

$$a(u, v) \leq C_0 \|u\|_V \|v\|_V, \quad a(v, v) \geq c_0 \|v\|_V^2, \quad (7)$$

for all u and v in V . We also assume the bilinear form is symmetric, i.e.,

$$a(u, v) = a(v, u) \quad (8)$$

for all u and v in V . Then for any given load f in H , there is a unique solution w in V of the variational equation $a(w, v) = (f, v)_H$ for all v in V .

The bilinear form a can be used to define an alternate ‘‘energy’’ inner product and norm on V by setting $(u, v)_E = a(u, v)$ and $\|v\|_E = (v, v)_E^{1/2}$. Equation (7) gives $c_0 \|v\|_V^2 \leq \|v\|_E^2 \leq C_0 \|v\|_V^2$ for all $v \in V$, i.e., the energy norm $\|\cdot\|_E$ is equivalent to $\|\cdot\|_V$.

We assume the measurement model is of the form $y = Cw + \eta$, where y is the given measurement in \mathbb{R}^p , η is the unknown measurement noise in \mathbb{R}^p , and C is a bounded linear mapping from V to \mathbb{R}^p . The measurement operator C can be written as

$$Cw = [C_1 w, C_2 w, \dots, C_p w]^T,$$

where each C_i is a bounded linear mapping from V to \mathbb{R} for $i = 1, \dots, p$. This framework also includes the situation where some or all of the C_i map H into \mathbb{R}^p . In this case, there is a c_i in H such that $C_i w = (c_i, w)_H$.

IV.B. Load Estimation Inverse Problem

With the above general framework in place, we consider the following inverse problem: given a measurement y , find the load f that produces that measurement.

Load Estimation Inverse Problem: For a given measurement y in \mathbb{R}^p and unknown measurement noise η in \mathbb{R}^p , find the load f in H such that $y = Cw + \eta$, and $a(w, v) = (f, v)_H$ for all $v \in V$.

The above inverse problem is ill-posed, i.e., there is not a unique load f that produces the given measurement y . In fact, there are infinitely many pairs $\{f, \eta\}$ that can produce y . This can be seen as follows. Pick *any* $f \in H$ and let $w \in V$ be the unique solution of $a(w, v) = (f, v)_H$ for all $v \in V$. Setting $\eta = y - Cw$ gives a pair $\{f, \eta\}$ that produces the given measurement y . The ill-posedness of the problem is a consequence of having only finitely many equations ($y = Cw + \eta$) and an infinite dimensional space ($H \times \mathbb{R}^p$) for the unknowns ($\{f, \eta\}$), i.e, the problem is underdetermined.

Due to the ill-posed nature of the inverse problem, we want a procedure to produce a *unique* load f that is, in some sense, a natural estimate. To do this, we use tools from the field of inverse problems involving compact linear operators over Hilbert spaces; see, e.g., references 14–16. We briefly outline the main ideas and leave the precise details for another work. First, let S be the solution operator for the variational equation $a(w, v) = (f, v)_H$ for all $v \in V$, i.e., for f given, $Sf = w$ if w in V solves the variational equation. Then we may write the measurement equation $y = Cw + \eta$ as

$$y = Kf + \eta, \quad K = CS. \quad (9)$$

There are many different methods of producing natural estimates for f in (9) given y with η unknown (see the above references). In this work, we use Tikhonov regularization to estimate the load f . For a given constant $\beta > 0$ and norm $\|\cdot\|_X$, the Tikhonov regularized estimate f is the unique minimizer of

$$E_{TR}(f) = \beta \|f\|_X^2 + \|y - Kf\|_{\mathbb{R}^p}^2.$$

In finite dimensions (i.e., f , y , and η are vectors and K is a matrix), under certain statistical assumptions the Tikhonov regularized estimate coincides with both the maximum a posteriori estimator and the minimum variance estimator (see, e.g., references [16, Chapter 4] and [15, page 78]); therefore, this is a natural estimate. We do not attempt to extend such equivalences to this infinite dimensional problem.

Even in the Hilbert space setting, the Tikhonov regularized estimate has a natural interpretation as the estimate of minimum norm. Furthermore, a noise estimate is included. Therefore, we consider the following equivalent problem, which follows from the above Tikhonov regularized problem by multiplying by β^{-1} and setting $\eta = y - Kf$ and $\alpha = \beta^{-1}$. We chose the the norm on the load f to be the energy norm $\|\cdot\|_E$ described in Section IV.A.

Minimum Norm Load Estimation Problem: For a given constant $\alpha > 0$ and a given measurement $y \in \mathbb{R}^p$, find the load f in V and the measurement noise η in \mathbb{R}^p minimizing

$$E(f, \eta) = \|f\|_E^2 + \alpha \|\eta\|_{\mathbb{R}^p}^2 \quad (10)$$

subject to $y = Cw + \eta$, and $a(w, v) = (f, v)_H$ for all $v \in V$.

For PDE problems, the E norm on the load f involves spatial derivatives. Therefore, the E norm penalizes loads with large gradients, and we can expect the minimizing load to be smoothly varying in space.

The positive constant α in the above problem is a user-controlled measure of the relative sizes of the load f and the noise η . For example, if α is large, then the estimated noise η will be small in order to minimize the energy $E(f, \eta)$. Furthermore, taking α to infinity will drive the magnitude of the estimated noise η to zero. Also, if we have a rough idea of the magnitude of the measurement noise, we can choose α in order to obtain a noise estimate near that specific magnitude. We comment further on the choice of α below.

The load estimation algorithm given below follows naturally from the solution of the above minimum norm problem.

Proposition 1. *Under the assumptions in Section IV.A, the unique solution $f \in V$ and $\eta \in \mathbb{R}^p$ of the above minimum norm problem (10) is given as follows:*

1. For $i = 1, \dots, p$, let $w_i \in V$ be the unique solution to the variational equation $a(w_i, v) = C_i v$ for all $v \in V$.

2. For $i = 1, \dots, p$, let $z_i \in V$ be the unique solution of the variational equation $a(z_i, v) = (w_i, v)_H$ for all $v \in V$.
3. Let $Q \in \mathbb{R}^{p \times p}$ be the matrix with ij entries $Q_{ij} = (z_j, z_i)_E = a(z_j, z_i)$.
4. Let $\xi \in \mathbb{R}^p$ be the unique solution of $(Q + \alpha^{-1}I)\xi = y$, where $I \in \mathbb{R}^{p \times p}$ is the identity matrix.
5. Then the unique solution is

$$f = \sum_{i=1}^p \xi_i z_i, \quad \eta = \alpha^{-1} \xi, \quad (11)$$

where ξ_i is the i th component of ξ .

The result can be proved by considering the solution of the Tikhonov regularized problem and applying the results in [17, page 580]. We provide the details elsewhere.

We now give the load estimation algorithm and discuss implementation details.

IV.C. Load Estimation Algorithm

The above proposition leads naturally to the following load and measurement noise estimation algorithm.

Load Estimation Algorithm: Let $y \in \mathbb{R}^p$ be a given measurement, and let $\delta > 0$ be a given estimate of the measurement noise magnitude.

1. Choose $\alpha > 0$.
 2. For $i = 1, \dots, p$, approximate (e.g., using finite elements) the unique solution $w_i \in V$ of the variational equation $a(w_i, v) = C_i v$ for all $v \in V$.
 3. For $i = 1, \dots, p$, approximate the unique solution $z_i \in V$ of the variational equation $a(z_i, v) = (w_i, v)_H$ for all $v \in V$.
 4. Form the $p \times p$ matrix Q by computing the bilinear form in the ij entries $Q_{ij} = (z_j, z_i)_E = a(z_j, z_i)$.
 5. Compute $\xi \in \mathbb{R}^p$, the unique solution of $(Q + \alpha^{-1}I)\xi = y$.
 6. Form the load estimate f and measurement noise estimate η in (11).
 7. If $\|\eta\|_{\mathbb{R}^p}$ is close enough to δ , stop. Otherwise, select a different α and repeat.
-

We now discuss a few points.

First, in steps 2 and 3 of the algorithm, one must solve $2p$ variational problems, where p is the number of distinct measurements (recall, the measurement vector y is in \mathbb{R}^p). This is the most computationally intensive portion in the algorithm, especially if the number of measurements is large.

It is important to note that this algorithm likely will provide better estimates for smoothly varying loads. As discussed above, the E norm penalizes large gradients in the load; thus, the algorithm will likely produce a smoothly varying load. Therefore, if the actual load is not smooth (i.e., it is in H but not in V), then we expect the load estimate to be less accurate since we are approximating a nonsmooth function by a smooth function.

Lastly, in the algorithm one must choose a parameter α , compute the load and noise estimate, and check if the noise estimate is of the expected magnitude. If the magnitude of the noise is not close to the expected size, then one must adjust α and repeat the computations. A good strategy for updating α will of course be crucial for the efficiency of the algorithm. We do not address this here. However, as mentioned previously, the above minimum norm problem is equivalent to the Tikhonov regularization of the inverse problem; therefore, existing regularization parameter selection methods for inverse problems (see, e.g., references 14, 16) can be employed here.

As discussed above, we first developed the problem and algorithm at the PDE level and then discretized as opposed to discretizing first and then developing the algorithm at the finite dimensional level. There are advantages and disadvantages to developing the algorithm at the PDE level and then discretizing. The

most obvious disadvantage to this approach is the up front mathematical work required to correctly pose the problem and obtain the algorithm. However we believe there are many potential advantages that are worth the up front cost:

- Any numerical method for solving the PDEs in steps 2 and 3 can be used in the above algorithm; specifically, we can use specialized discretizations, any computational grid, any existing linear solvers, adaptive error estimators and mesh refinement, multigrid methods, powerful existing codes, etc. Furthermore, when using existing codes, the algorithm only requires the approximate solutions of PDEs and does not explicitly require access to any matrices. If we discretize the problem first, then we may lose the ability to use many of the above techniques.
- Developing the problem and the algorithm at the PDE level allowed us to obtain the exact form of the load estimate (11). Therefore, there was no need to discretize the unknown load in advance as was done, e.g., in references 5–9, 11. Li⁶ showed that this approach led to widely differing load estimates depending on the basis used for the load discretization. There was no way to tell in advance whether a particular choice of basis would lead to a successful load estimate. This was not an issue in this work.
- We can obtain guarantees of accuracy and convergence to the true load estimate in (11) given by the algorithm at the PDE level. Therefore, if the computations in the algorithm are performed with sufficient accuracy, then the output of the algorithm will be sufficiently close to the true estimate. This is true regardless of discretization scheme, etc. Thus, different computational approaches for the computations in steps 2 and 3 should yield roughly the same output.
- Developing the solution to the minimum norm problem at the PDE level allowed us to avoid the singular value decomposition usually required for the solution of the Tikhonov regularized inverse problem; this led to a more efficient algorithm.
- As mentioned previously, the algorithm is applicable to a wide class of elliptic PDE systems. One need only change the Hilbert spaces and bilinear form to utilize the algorithm for a different problem. Furthermore, we anticipate a similar solution strategy will yield load estimation algorithms for similar problems that do not fall into the general framework considered here.

V. Finite Element Implementation and Details

Here we provide numerical details on the application of the load estimation algorithm (presented in Section IV.C) to the linear membrane problem described above. Throughout, all PDE's are solved with the finite element method.

Step 1 - Compute or Acquire Measurements

In experimental settings, measurements $y \in \mathbb{R}^p$ are acquired from sensors. For computational tests, we must compute the measurements $y \in \mathbb{R}^p$, where $p = 2m$ before hand. To this end, we approximate w with the finite element method.

Let w be approximated as

$$w(x, y) \approx \hat{w}(x, y) = \sum_{i=1}^N a_i \phi_i(x, y). \quad (12)$$

where each $\phi_i \in V$. The substitution of (12) into (6) leads to the following matrix equation

$$\mathbf{K} \mathbf{a} = \mathbf{F}, \quad (13)$$

where

$$\mathbf{K} = (N_{11} \phi_{i,x} \phi_{j,x}) + (N_{12} \phi_{i,x} \phi_{j,y}) + (N_{12} \phi_{i,y} \phi_{j,x}) + (N_{22} \phi_{i,y} \phi_{j,y}), \text{ and} \quad (14)$$

$$\mathbf{F} = (f, \phi_i)$$

for $i, j = 1, \dots, N$, where (\cdot, \cdot) represents the L^2 inner product. Solving the linear algebraic equation (13) for \mathbf{a} , the measurements (4) are computed as

$$\mathbf{y} = \mathbf{D} \mathbf{a} + \eta, \quad (15)$$

where $\mathbf{D}_{kj} = (g_k, \phi_{j,x})$ for $k = 1, \dots, m$ and $j = 1, \dots, N$, and $\mathbf{D}_{kj} = (g_k, \phi_{j,y})$ for $k = m + 1, \dots, 2m = p$ and $j = 1, \dots, N$.

Step 2 - Solve $Aw_i = C_i$ and $Az_i = w_i$

Next, we approximate the solution of the variational equations in steps 2 and 3 of the algorithm. The approximation of solutions to $a(w_k, v) = C_k v$ for $k = 1, \dots, p$ is similar to the membrane problem described in the previous step. Let w_k and z_k be approximated as, $\sum_{i=1}^N b_{ki} \phi_i$ and $\sum_{i=1}^N d_{ki} \phi_i$, respectively. Then for $k = 1, \dots, p$ we may compute the vectors b_k and d_k by solving

$$\mathbf{K} b_k = \mathbf{D}_k,$$

where \mathbf{D}_k is the k th column of the matrix \mathbf{D} defined above, and

$$\mathbf{K} d_k = b_k.$$

Step 3 - For $k, \ell = 1, \dots, p$, compute $Q_{k\ell} = (z_k, z_\ell)_E$

We compute the $p \times p$ matrix Q in step 4 of the algorithm as follows. Recall from step 2 of the algorithm that $(z_j, v)_E = a(z_j, v) = (w_j, v)_H$. Therefore, $(z_k, z_\ell)_E = (w_k, z_\ell)$. The substitution of (12) into Q leads to

$$Q_{k\ell} = \sum_{i,j=1}^N d_{ki} (\phi_i, \phi_j) b_{\ell j}. \quad (16)$$

In matrix form (16) becomes

$$Q = \mathbf{d}^T \mathbf{M} \mathbf{b} \quad (17)$$

where \mathbf{d} is an $N \times p$ matrix with columns d_k for $k = 1, \dots, p$, \mathbf{b} is an $N \times m$ matrix with columns b_p for $k = 1, \dots, p$, and \mathbf{M} is the $N \times N$ mass matrix with ij entries (ϕ_i, ϕ_j) .

VI. Numerical Results

We consider the following three arrays of measurements (Figures 5, 6, and 7). The measurement region

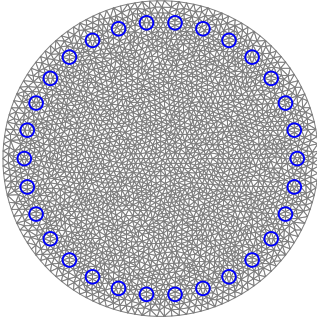


Figure 5. Sensor array A

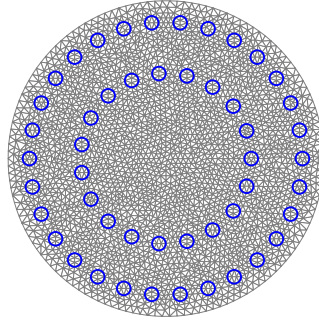


Figure 6. Sensor array B

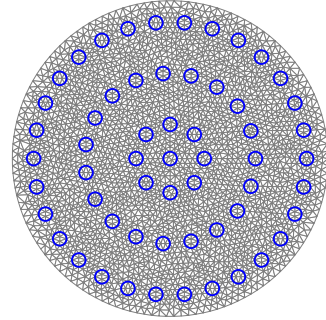


Figure 7. Sensor array C

shape and configuration was chosen to provide an increasing amount of measurements going from array A to B and B to C. Since the location (and region shape) of any measurement will contribute differently to a load estimation, we make array A a subset of B and B a subset of C. As a result, we ensure that the overall amount of information increases with sensor number.

The measurement regions are superimposed on the single finite element mesh used throughout this analysis. The FE mesh is composed of 3031 triangular elements having nodes specially aligned with the sensor boundaries, to avoid slow FE convergence.¹⁸ We test each measurement array with the following set

of distributed loads (Figure 8)

$$\begin{aligned}
 \text{Load I: } f &= (x^2 + y^2 - R^2) \times 10^{-5} \\
 \text{Load II: } f &= (x^2 + y^2 - R^2) \sin(\pi x/40) \cos(\pi y/45) \times 10^{-5} \\
 \text{Load III: } f &= (x^2 + y^2 - R^2) [(x + 5)^2 + (y + 14)^2] \times 10^{-8},
 \end{aligned}
 \tag{18}$$

where R is the outer membrane radius (taken here as $R = 46.25\text{mm}$) and the exponents were chosen in the spirit of ensuring the physical validity of the linear membrane model. We also specify Young's modulus as $E = 2.2 \times 10^3 \text{ Pa}$, Poisson's ratio as $\nu = .45$, and the membrane thickness as $t = 0.1 \text{ mm}$. Note that each

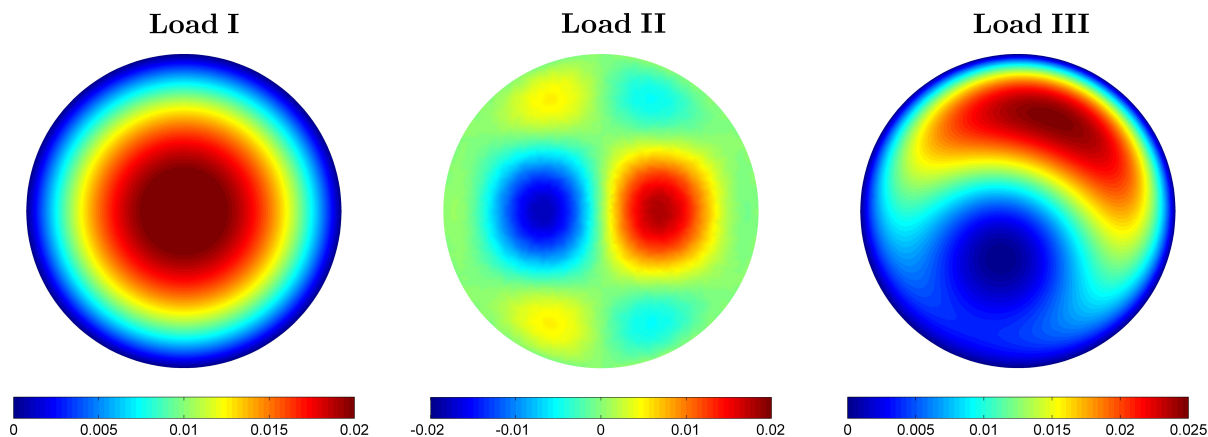


Figure 8. From left to right, distributed loads I, II, and III chosen for this analysis

load has zero value on the domain boundary. This ensures that f satisfies the zero boundary conditions in (1) (i.e., f conforms in V as posed in the minimum norm problem (10)).

VI.A. Load estimates without measurement noise

Figure 9 contains E -norm estimates for loads I, II and III for each measurement array A, B and C, without noise ($\eta = 0, \alpha = 1 \times 10^{20}$), where the particular load-array combination is indicated at the top of each plot.

As expected, estimation accuracy improves as more information or measurements are added, with the greatest improvements observed going from array A to B for loads II and III. The addition of the center measurements in array C appears to have little influence on the estimation accuracy. We quantify the accuracy of each estimate above with the following relative error measure

$$\text{error} = \frac{\|f - f_{est}\|_{L^2}}{\|f\|_{L^2}}.
 \tag{19}$$

Table 1 lists the relative error values (19) for each load and measurement pair.

Table 1. Accuracy for each load estimate and measurement array with 0% noise

	Load I	Load II	Load III
Array A	0.0241	0.5144	0.3958
Array B	0.0136	0.0720	0.0946
Array C	0.0134	0.0492	0.0949

Note the disparate and redundant information contained in the measurements for each load. With array A, the load estimate I is essentially converged, while loads II and III are not. Adding 19 measurements (going from array A to B) reduces error by 1.0% for load I, 44% for load II, and 30% for load III. Thus, for load estimate I, the information contained in array II was either redundant had little value, or both. Conversely, array B contained a significant amount of new information for loads II and III. For all loads,

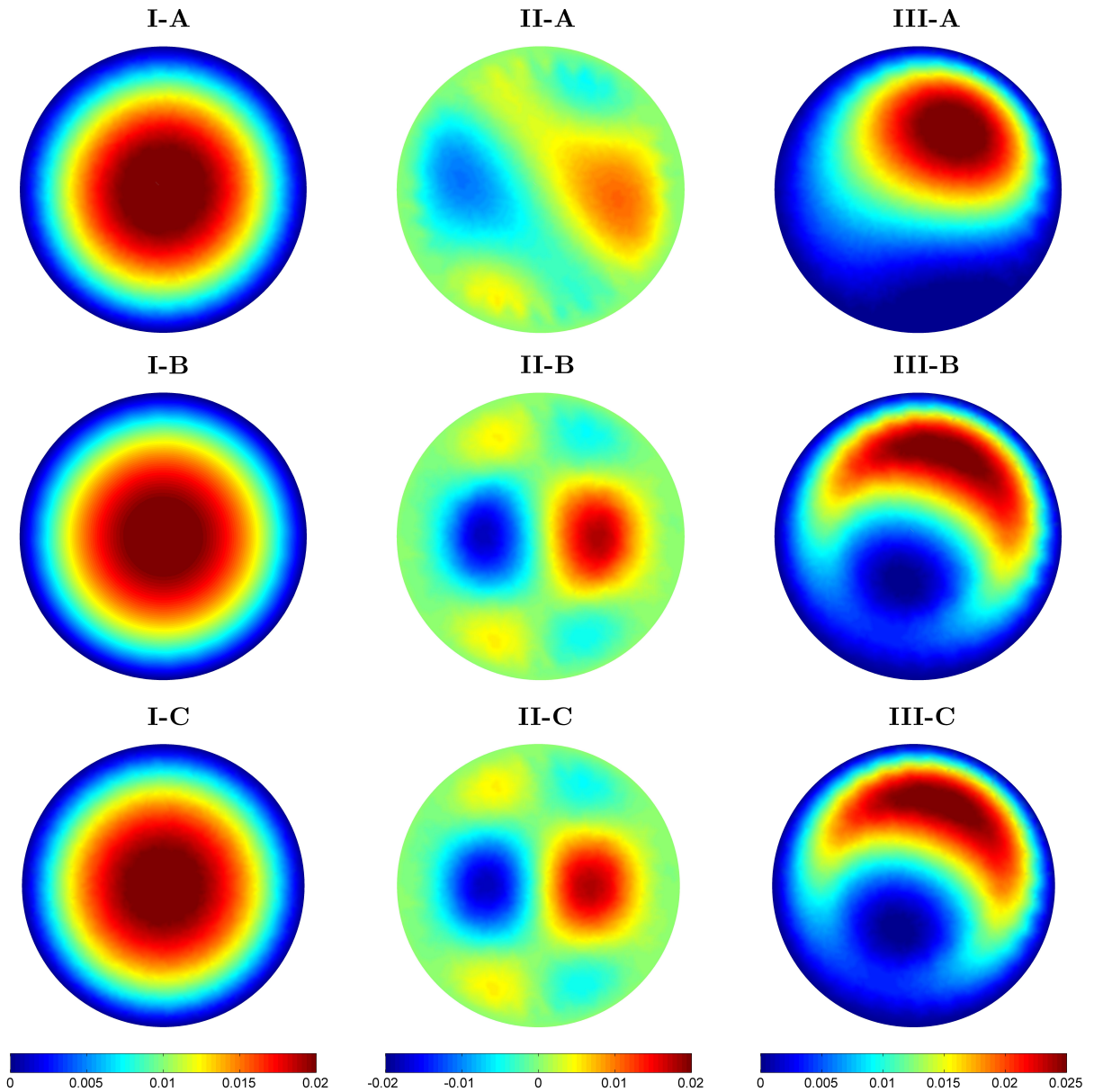


Figure 9. Estimates for loads I,II, and III for measurement arrays A, B, and C

little improvement in accuracy was realized going from array B to C. In fact, the estimate accuracy of load III decreased by 0.03%. A likely source for this slight decrease in accuracy is numerical error in the finite element approximation. Additionally, while adding information seems to improve estimation accuracy in general, we have no guarantees that estimates will converge monotonically.

VI.B. Load estimation with measurement noise

We now consider the case where noise is added to the measurement signal. We further denote measurement noise as $X\%$, where each measurement signal, y_i for $i = 1, \dots, 2m$, receives an added noise signal η_i randomly chosen over the interval $[-Xy/100, Xy/100]$.

Recall that in the load estimation algorithm (Section IV.C), we obtain estimates of the noise, η , by choosing the parameter α such that $\|\eta\|_{\mathbb{R}^p} \approx \delta$, where δ is a known estimate of the measurement noise magnitude. As expected and illustrated in Figures 10 and 11, we find that load estimate accuracy improves with accurate noise estimation ($\|\eta\|_{\mathbb{R}^p}$ approaches δ).

In Figures 10 and 11, the maximum load estimate accuracies (roughly 3.5% and 5.0%, respectively) occur

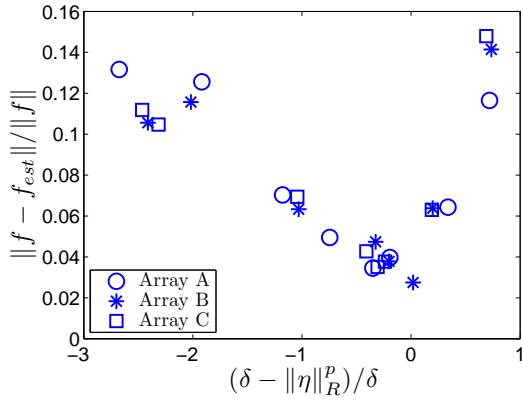


Figure 10. Load I estimate accuracy vs 5% noise estimate accuracy

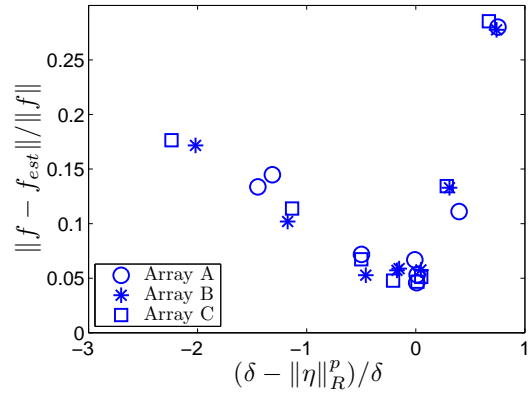


Figure 11. Load I estimate accuracy vs 10% noise estimate accuracy

near $\delta - \|\eta\|_{R^p} = 0$. Underestimated noise ($\delta - \|\eta\|_{R^p} > 0$, α is larger than its optimal value) leads to load estimates with unaccounted for measurement noise. Note that load estimate error increases at a significantly larger rate for underestimated noise, than overestimated noise ($\delta - \|\eta\|_{R^p} < 0$, α is smaller than optimal). As $\alpha \rightarrow 0$, the minimization of $\|f\|_E$ in $E(f, \eta)$ becomes overemphasized to the point where f is driven to zero everywhere.

The effect of α on estimate accuracy may be best illustrated through visualization of the actual load estimates. Figures 12-15 are estimates of Load I with Array A and 10% measurement noise. Moving from

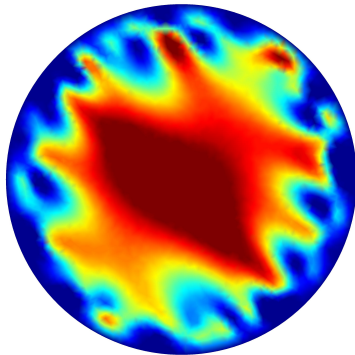


Figure 12. $\alpha = 1 \times 10^0$, $(\delta - \|\eta\|_{R^p})/\delta = 0.98$, Array A, 10% noise

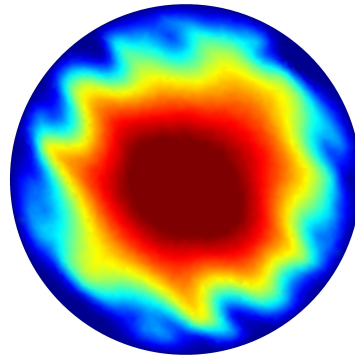


Figure 13. $\alpha = 1 \times 10^{-1}$, $(\delta - \|\eta\|_{R^p})/\delta = 0.60$, Array A, 10% noise

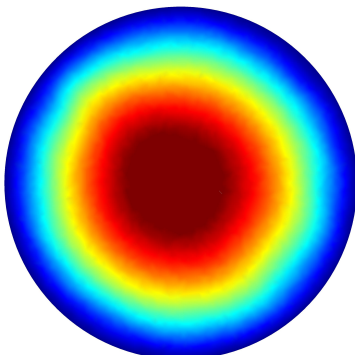


Figure 14. $\alpha = 1 \times 10^{-2}$, $(\delta - \|\eta\|_{R^p})/\delta = 2.0e - 4$, Array A, 10% noise

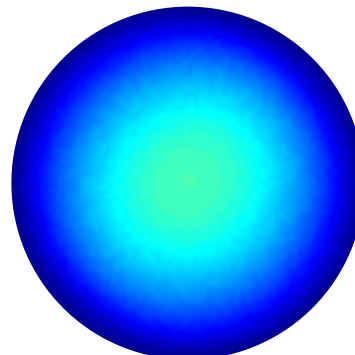
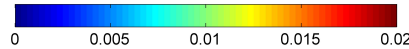
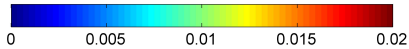


Figure 15. $\alpha = 1 \times 10^{-3}$, $(\delta - \|\eta\|_{R^p})/\delta = -5.9$, Array A, 10% noise



top to bottom and left to right, α decreases from 1×10^0 to 1×10^{-4} . Figure 12 shows a corrupted load estimate due to underestimated measurement noise. Noise is better estimated, although still underestimated, in Figure 15, which results in an estimate more closely resembling load I. The best estimate, among the four figures, occurs when $\alpha = 1 \times 10^{-2}$ with a noise estimate error of 0.02%. The effect of a largely overestimated measurement is shown in Figure (15). Clearly, obtaining the most accurate load estimates from noisy measurements will require some tuning of the regularization parameter, α . Selection methods α are briefly mentioned in Section IV.C with references.

VII. Summary

In the same way that we can feel the forces on our limbs when we walk, swim, or hold our arms out the window of a moving car, we anticipate that natural flyers feel the aerodynamic loads on their wings and that this sense plays a significant role in their agile yet stable flight. To bring this capability of agile flight to micro air vehicles, we looked at developing techniques to determine aerodynamic loading with ultimate goal of online, real-time estimation for flight control system designs.

In this study, we developed a general algorithm for the estimation of steady distributed loads on linear structures from noisy deformation-based measurements. Compared to existing load estimation routines, the algorithm developed here is discretization independent; leads to the exact form of the load estimate; enables guarantees of accuracy and convergence to the true load estimate at the continuous level; and is valid for a wide class of PDE systems. Drawbacks of this method from existing techniques include up front mathematical work to correctly pose the problem and computational cost.

Because of the proliferation of membrane wings on today's state-of-the-art MAVs, the steady load estimation algorithm developed herein was applied to a linear membrane test problem. Our numerical results showed that simple measurement configurations lead to highly accurate load estimates. Additionally, with the proper choice of the regularization parameter (α), we demonstrated accurate load estimates despite noisy measurements.

VIII. Future Work

Measurement optimization and strategy

Minimizing the computational cost of load estimates while maintaining sufficient accuracy leads us to consider the value of measurements. As discussed in Section VI, measurements may be redundant or be placed in a location of little value. To avoid unnecessary computational effort associated with processing such measurements, one may consider an optimization of measurement placement, shape, etc. Additionally, although not essential, optimizations tailored toward an *a-priori* load characterization may lead to the most effective configurations.

Even with an optimized configuration, load scenarios will likely occur where measurements are redundant or have little value. As an alternative to (or in combination with) optimized measurements, cost may be further reduced by filtering unimportant information prior to the estimation routine. Conceivably, such filtering could be used with dense sensor arrays. Further, a surplus of sensors may lead to a more robust system to sensor failure. We anticipate that both measurement optimization and information filtering strategies are existing topics of research. We will pursue such topics in the future.

Computational cost and applications

For the load estimation routine developed herein, the cost associated with solving $4m$ PDEs (2 PDEs per measurement \times 2 measurements per region \times m regions) poses questions of computational tractability, especially for control applications. As discussed above, measurement optimization and filtering are potential options for less costly implementations. Additional cost savings may be realized through model reduction, such as low-order Galerkin truncations with proper orthogonal decomposition. Given the limited power supplies and computational resources currently available to MAV platforms, developing efficient PDE-based algorithms for MAVs appears to be a challenge.

Future studies include developing methods for unsteady load estimation. Preliminary investigations into unsteady estimation methods indicate that the extension from the steady estimation problem is not straightforward. We note that, all studies referenced herein were for steady problems and, to our knowledge;

this capability has not been developed. Furthermore, the unsteady structural dynamics of compliant aircraft may require unsteady methods for nonlinear structures.

Sensor/Actuator development

Moving toward the physical application of load estimation methods, the actual sensors must be considered. The development, design, and characterization of high sensitivity sensors, suitable for the purposes described herein, is a topic of a concurrent research effort within the Air Force Research Laboratory Materials Directorate. Advanced materials such as carbon nano tubes and graphene are currently being explored and characterized as potential sensors¹⁹ along with conventional strain sensor technology. Beyond measurement algorithms and sensor development, sensor integration in MAV platforms is an engineering challenge.

Advanced actuators or flow effectors will need to be addressed as well. Conventional movement of aerodynamic surfaces such as elevators and ailerons may be insufficient for agile flight control. Bio-inspired concepts for flight control include the ability to change shape and change structural stiffness.

The culmination of advanced sensors, actuators, and control designs is believed necessary to truly achieve the proficiency of flight exhibited by natural flyers.

References

- ¹W. Shyy, Y. Lian, J. Tang, D. Viieru, and H. Liu, *Aerodynamics of low Reynolds number flyers*. Cambridge University Press, 2008.
- ²T. Muller, "An overview of micro air vehicle aerodynamics," in *Fixed and flapping wing aerodynamics for micro air vehicle applications*, pp. 1–9, AIAA, 2001.
- ³M. Ol, G. Parker, G. Abate, and J. Evers, "Flight control and performance challenges for MAVs in complex environments," in *AIAA Guidance, Navigation, and Control Conference*, 2008. AIAA Paper Number 2008-6508.
- ⁴R. Thompson, J. Evers, and K. Stewart, "Attitude control augmentation using wing load sensing - A biologically motivated strategy," in *AIAA Atmospheric Flight Mechanics Conference*, 2010.
- ⁵J. Chock and R. Kapania, "Load updating for finite element models," *AIAA Journal*, vol. 41, pp. 1667–1673, 2003.
- ⁶J. Li and R. Kapania, "Load updating for nonlinear finite element models," *AIAA Journal*, vol. 45, pp. 1444–1458, 2007.
- ⁷A. Maniatty, N. Zabaras, and K. Stelson, "Finite element analysis of some inverse elasticity problems," *Journal of Engineering Mechanics*, vol. 115, pp. 1303–1317, 1989.
- ⁸C. Coates and P. Thamburaj, "Inverse method using finite strain measurements to determine flight load distribution," *Journal of Aircraft*, vol. 45, pp. 366–370, 2008.
- ⁹S. Shkarayev, R. Krashantisa, and A. Tessler, "An inverse interpolation method utilizing in-flight strain measurements for determining loads and structural response of aerospace vehicles," in *Structural Health Monitoring: The Demands and Challenges, Proceedings of 3rd International Workshop on Structural Health Monitoring*, 2001.
- ¹⁰J. White, D. Douglas, and M. Rumsey, "Operational load estimation of a smart wind turbine rotor blade," in *Health Monitoring of Structural and Biological Systems*, 2009.
- ¹¹B. Stanford, R. Albertani, and P. Ifju, "Inverse methods to determine the aerodynamic forces on a membrane wing," in *48th Structures, Structural Dynamics, and Materials Conference*, 2007. AIAA Paper Number 2007-1984.
- ¹²B. Stanford and P. Ifju, "The validity range of low fidelity structural membrane models," *Exp Mech*, vol. 48, pp. 697–711, 2008.
- ¹³H. T. Banks, R. C. Smith, and Y. Wang, *Smart Material Structures: Modeling, Estimation and Control*. Wiley, 1996.
- ¹⁴H. W. Engl, M. Hanke, and A. Neubauer, *Regularization of Inverse Problems*, vol. 375 of *Mathematics and its Applications*. Dordrecht: Kluwer Academic Publishers Group, 1996.
- ¹⁵J. Kaipio and E. Somersalo, *Statistical and Computational Inverse Problems*. New York: Springer-Verlag, 2005.
- ¹⁶C. R. Vogel, *Computational Methods for Inverse Problems*. Philadelphia, PA: SIAM, 2002.
- ¹⁷M. Bertero, C. De Mol, and E. R. Pike, "Linear inverse problems with discrete data. II. Stability and regularisation," *Inverse Problems*, vol. 4, no. 3, pp. 573–594, 1988.
- ¹⁸G. Strang and G. Fix, *An Analysis of the Finite Element Method*. Wellesley-Cambridge Press, 2008.
- ¹⁹M. Maschmann, Q. Zhang, F. Du, L. Dai, and J. Baur, "Height-dependent foam-like behavior of carbon nanotube arrays." Submitted to the journal *Small*.